Increased collagen within ~~Fibrosis of~~ the transverse tubules in human heart failure

David J Crossman[1], PhD; Xin Shen[1], PhD; Mia Jüllig[2], PhD; Michelle Munro[1], PhD; Yufeng Hou[1], PhD; Martin Middleditch[2],BSc; Darshan Shrestha[1], BSc, Amy Li[3], PhD; Sean Lal[3], MD; Cristobal G. dos Remedios[3], DSc; David Baddeley[4], PhD; Peter N Ruygrok[5], MD, PhD; Christian Soeller, PhD[1,6]

[1]Department of Physiology, University of Auckland, Auckland, New Zealand; [2]School of Biological Sciences, University of Auckland, Auckland, New Zealand; [3]Bosch Institute, University of Sydney, Sydney, Australia; [4]Department of Cell Biology, Yale University, New Haven, USA; [5]Department of Cardiology, Auckland City Hospital, New Zealand; [6]Living Systems Institute and Biomedical Physics, University of Exeter, UK.

Correspondence:
Dr David Crossman
Department of Physiology, University of Auckland, Private Bag 92019, Auckland 1142, New Zealand, Tel: + 64 9 3737599 xt 89964, Fax: + 64 9 373 7499.
Email: d.crossman@auckland.ac.nz
Prof Christian Soeller
Biomedical Physics, University of Exeter, Stocker Road, Exeter EX4 4qL, UK. Tel: + 44 1392 726608, Fax: + 44 1392 264111.
Email: c.soeller@exeter.ac.uk

Abstract

Aims: In heart failure transverse-tubule (t-tubule) remodelling disrupts calcium release, and contraction. T-tubules in human failing hearts exhibit increased labelling by wheat germ agglutinin (WGA), a lectin that binds to the dystrophin-associated glycoprotein complex. We hypothesized changes in this complex may explain the increased WGA labelling and contribute to t-tubule remodelling in the failing human heart. In this study we sought to identify the molecules responsible for this increased WGA labelling.

Methods and Results: Confocal and super resolution fluorescence microscopy and proteomic analyses were used to quantify left ventricle samples from healthy donors and patients with idiopathic dilated cardiomyopathy (IDCM). Confocal microscopy demonstrated both WGA and dystrophin were located at t-tubules. Super resolution microscopy revealed that WGA labelling of t-tubules is largely located within the lumen while dystrophin was restricted to near the sarcolemma. Western blots probed with WGA reveal a 5.7-fold increase in a 140 kDa band in IDCM. Mass spectrometry identified this band as type VI collagen (Col-VI) comprised of α1(VI), α2(VI), and α3(VI) chains. Pertinently, mutations in Col-VI cause muscular dystrophy. Western blotting identified a 2.4 fold increased expression and 3.2 fold increased WGA binding of Col-VI in IDCM. Confocal images reveal that Col-VI is located in the t-tubules and that their diameter increased in the IDCM samples. Super resolution imaging revealed Col-VI was restricted to the t-tubule lumen where increases were associated with displacement in the sarcolemma as identified from dystrophin labelling. Samples were also labelled for type I, III, and IV collagen. Both confocal and super resolution imaging identified that these collagens were also present within t-tubule lumen.

Conclusions: Increased expression and labelling of collagen in IDCM samples indicates fibrosis may contribute to t-tubule remodelling in human heart failure.

Key Words: Human heart failure; Idiopathic dilated cardiomyopathy; Transverse tubules; Type VI collagen; Super resolution

Introduction

Transverse tubules (t-tubules) are extensions of the plasma membrane that penetrate the cardiac myocyte, forming electrical connections between the surface membrane and the sarcoplasmic reticulum (SR) called cardiac junctions that enable synchronized calcium release and hence contraction[1,2]. These junctions constitute a nanoscale interface between the plasma and SR membranes and their remodelling appears to play a major role in the pathogenesis of heart failure[3,4]. Experiments in animal models have demonstrated that t-tubule structure becomes disrupted in heart failure leading to disrupted SR calcium release, and reducing contractile function[5–11]. Furthermore, similar changes appear to contribute to the loss of contractile function in human heart failure[12–19]. Intracellular proteins that align plasma and SR membranes have been implicated in t-tubule remodelling[20–26]. However, our previous work suggested that the extracellular matrix may also be directly involved. We have previously documented enlargement and disarrangement of t-tubules in the failing human heart using confocal imaging of tissue sections labelled with wheat germ agglutinin (WGA)[17,18]. WGA is thought to bind to glycosylated proteins in the extra cellular matrix including those of the dystrophin glycoprotein complex (DGC)[27]. This complex is critical to normal muscle function. Mutations in the genes encoding this complex lead to muscular dystrophy and to heart failure in older patients[28,29]. The DGC forms a mechanical connection between the cytoskeleton and the extracellular matrix (ECM) and is therefore essential for transmitting force during muscle contraction[29]. Changes in dystrophin have been observed in end-stage human heart failure[30] and dystrophin remodelling is associated with hypertrophied t-tubules in the failing human heart[31].

We used liquid chromatography tandem mass spectrometry (LC MS/MS) to investigate the increase in WGA labelling and were able to identify a major component originating from type VI collagen (Col-VI) a collagen that when mutated can induce muscular dystrophy[32]. We investigated Col-VI and several other collagens (type IV (Col-IV) type III (Col-III) and type I (Col-I)) in human tissue samples and detected all of these collagens in the t-tubules using a combination of confocal and novel super-resolution methods. Our data support a new hypothesis that cardiac fibrosis not only contributes to expansion of the interstitial space but also to t-tubule remodelling in human heart failure.

Methods

Human heart samples

Human cardiac tissue from failing hearts was obtained from the Auckland City Hospital transplant program. Non-failing human LV samples from organ donors were obtained from Organ Donation New Zealand, and from the University of Sydney in collaboration with St Vincent's Hospital, Sydney. All human tissue was obtained with written and informed consent from transplant recipients or families of organ donors in accordance to the declaration of Helsinki, institutional guidelines as approved by the Health and Disability Ethics Committees New Zealand (NTY/05/08/050/AM05), Human Research Ethics Committees at University of Sydney (2012/2814), and St Vincent's Hospital (H03/118). Details of the heart samples are presented in Table 1. Note that the non-failing samples and IDCM samples have broadly similar age and sex distribution. For immunohistochemistry LV tissues were fixed in 2% paraformaldehyde in PBS for 1 hour 4°C, cryoprotected in 30% sucrose, frozen with liquid nitrogen chilled isopentane, and stored at −80°C. Samples for protein work were preserved in RNA later overnight at 4°C and then frozen in liquid nitrogen chilled isopentane and stored at −80°C. Samples from Sydney University were frozen directly in liquid nitrogen.

Table I. Donor and Patient characteristics.

Donor		IDCM					
Age, y	Sex	Age, y	Sex	NYHA	LVEF, %	LVEDD, mm	LVESD, mm
62	F	57	F	III	15	72	65
57	F	54	M	III-IV	18	80	74
56	M	52	M	III-IV	17	67	61
54	F	50	M	II on LVAD	18	93	
48	F	49	F	III	21	74	64
53	M	48	F	III-IV	18	69	65
42	F	42	F	I on LVAD	25	76	65
19	M	21	M	III	14	90	84
		21	M	III-IV	19	76	68
		18	M	IV	15	68	65
		17	F	III-IV	20	98	82

NYHA, New York Heart Association functional classification. LVAD, left ventricle assist device. LVEF, left ventricle ejection fraction. LVEDD, left ventricle end diastolic diameter. LVESD, left ventricle end systolic diameter.

Immunofluorescence labelling

Frozen sections (10 µm) were mounted on coverslips, permeabilized with 1% triton X100 in PBS for 15 minutes, and blocked with FX signal enhancer (ThermoFisher) for 1 hour. For WGA and dystrophin labelling, sections were incubated with rabbit antibody against dystrophin (1:100, AB15277, Abcam) overnight at 4 °C. For confocal imaging, sections were incubated with goat anti-rabbit Alexa Fluor 488 antibody and WGA Alexa Fluor 594 (both 1:100, Life Technologies). For super resolution imaging sections were incubated with anti-

rabbit Alexa Fluor 750 antibody (1:100) and WGA Alexa Fluor 680/488 (1:125 and 1:500 respectively). Alexa Fluor 488 aided visualisation by eye. For collagen and dystrophin labelling, permeabilized sections were incubated with respective rabbit antibodies against collagen (1:100, Col-VI, AB6588, Col-IV, AB6586, Col-III, AB7778, Col-I, AB34710, from Abcam) and mouse antibodies against dystrophin (1:100, D8168, Sigma) overnight at 4 °C. For confocal imaging sections were incubated with goat anti-rabbit Alexa Fluor 488 antibody and goat anti-mouse Alexa Fluor 594 (both 1:100, Life Technologies, USA). For super resolution imaging sections were incubated instead with goat anti-rabbit Alexa Fluor 680/488 (1:125 and 1:500 respectively) and goat anti-mouse Alexa Fluor 750 antibody (1:100). Note antibody solutions were diluted in 1% BSA, 0.05% triton X100, 0.05% NaN_3 in PBS. For confocal assessment of fibroblast numbers permeabilized tissue sections were incubated with rabbit antibody against Col-VI (1:100 AB6588) and mouse antibody against vimentin (1:500 V 6630, Sigma) overnight at 4 °C. Sections were then incubated with goat anti-rabbit Alexa Fluor 488 (1:100), goat anti-mouse Alexa Fluor 568 (1:100), DAPI (0.01 mg/ml), and phalloidin (1:50, all from Life Technologies, USA),

Confocal Imaging and image processing

Samples were mounted in 90% glycerol in PBS. Confocal images were obtained on a Zeiss LSM 710 inverted confocal microscope. For t-tubule analysis 3D image stacks were collected with 63x NA 1.4 oil-immersion objective (80 x 80 x 300 nm pixel spacing). Image stacks were deconvolved as previously described[33]. T-tubule widths were estimated by obtaining a perpendicular line profile (400 nm wide) and fitting a Gaussian function using ImageJ and calculating the full width half maximum (FWHM)[17]. For assessment of tissue fibrosis three 2D images 425 by 425 μm were collected for each heart with 20x 0.8 NA air objective at pixel spacing of 200 nm. Images were median filtered (2 x 2 pixel kernel) to reduce noise followed by thresholding at the modal intensity plus one standard deviation. Total percent of the resulting mask was use as metric of labelling area (Supplementary Figure 1). For the assessment Col-VI positive fibroblasts, cell numbers were counted in five 2D images 169 x 169 μm collected from each heart with a 63x NA 1.4 oil objective. Fibroblasts were identified from vimentin labelling a cytoskeletal protein found fibroblasts but not myocytes[34]. A fibroblast was considered Col-VI positive if the vimentin labelling overlapped or colocalised with Col-VI labelling and the cell had a visible nucleus located in the interstitial space.

Super-Resolution Imaging (dSTORM)

Samples were mounted in dSTORM imaging media consisting of 90% glycerol and 10 mM MEA in PBS[35]. Sections were then imaged on a Nikon TE2000 inverted total internal reflection fluorescence (TIRF) microscope modified for localisation microscopy as previously described[36]. Briefly, a solid-state 671 nm laser (Viasho, China) was focused onto the sample via a 60x 1.49NA oil-immersion TIRF objective (Nikon) in a highly inclined light sheet[37]. Emission light was passed through a Q680LP dichroic mirror (Chroma Technology) and an XF3104-690ALP emission filter (Omega optical) prior to being split into two spectral channels. dSTORM optical sections of transversely orientated myocytes were acquired for 20,000-40,000 frames at rate of 50 ms per frame. The emission light for the two channels was recorded onto the two halves of the cooled EM-CCD chip of an IXon DV887DCS-BV camera (Andor Technology, Belfast).

dSTORM Image analysis

Single molecule events were localised and spectrally separated by analysing recorded image stack using custom-written algorithms implemented in Python[35,36]. Point data of each fluorophore is rendered onto 5 nm × 5 nm/pixel 2D greyscale TIFF image using jittered triangulation[38]. T-tubule widths were estimated from perpendicular line profiles. WGA and ColVI widths were estimated from calculating FWHM using fitted Gaussian parameters. For dystrophin where a double row of labelling was visible a Gaussian was fitted to each row and widths estimated from respective FWHM as illustrated in Supplementary Figure 2.

Western Blot and LC-MS/MS

Western blot and LC-MS/MS were carried out with standard protocols as described in the supplementary material and Supplementary Figure 3. Briefly, homogenates of heart tissue were separated by SDS-PAGE, transferred to PVDF or nitrocellulose membranes. WGA positive proteins were detected by incubating blots with WGA Alexa Fluor 680 conjugate overnight. For mass spectrometry detection of Col-VI the ~140 kda WGA positive band was excised, trypsin digested and analysed by LCMS/MS (QSTAR XL) with the resulting spectra searched against NCBI's human protein database using Mascot software. Western for Col-VI involved incubating blots with Col-VI antibody (AB6588, Abcam raised against full length alpha-1(VI) chain) overnight followed by secondary antibodies labelled with Alexa Fluor 647 for 1 hour.

Col-VI alpha chain analysis

Details of the analysis are described in the supplementary methods. Briefly, homogenates of heart tissue were separated by SDS-PAGE. The ~140 kDa region from the gel was excised, trypsin digested and analysed by LCMS/MS (Sciex Triple TOF 6600) with the resulting spectra searched against NCBI's human protein database using Mascot software to detect Col-VI alpha chains.

Statistics

Values presented are means ± SEM. Differences between sample means were tested with either student's t-test or an unequal variance t-test (IBM SPSS Statistics version 22) with $p<0.05$ considered significant. The Bonferroni method was used to adjust for multiple comparisons.

Results

WGA and dystrophin labelling of t-tubules

Confocal imaging of donor human ventricle showed that the sarcolemma and t-tubules are both labelled with WGA and dystrophin antibodies (Figure 1A). However WGA also labels the ECM whereas antibodies to dystrophin are restricted to near the sarcolemma, consistent with the intracellular location of dystrophins[29]. For the larger donor t-tubules there is a double row of dystrophin labelling that flanks WGA (Figure 1A insert) consistent with two opposing sides of the curved t-tubule membrane. However, for most t-tubules, WGA and dystrophin labelling cannot be resolved due to the confocal optical resolution limit (~250 nm). In diseased cardiac tissue a noticeable increase in WGA labelling of the ECM, cell surface and t-tubules was observed. In the IDCM LV samples, dystrophin labelling was similarly restricted to the cell surface and t-tubules (Figure 1B). Many of these were noticeably dilated with double rows of dystrophin flanking WGA labelling (Figure 1B insert). As we and others

observed before many failing myocytes have a reduced number or even an absence of t-tubules[17,18,31].

T-tubule diameters were quantified by their full width half maximum (FWHM) estimated from Gaussian function fitted to the intensity profile of t-tubules in confocal images of WGA and dystrophin. The distribution of widths for 150 donor tissue t-tubules (from 5 hearts) and 150 diseased t-tubules (from 5 explanted hearts) are presented in Figure 1C. This analysis demonstrates diseased t-tubules are wider and have a larger distribution of diameters than donor t-tubules, consistent with our previous report[17]. The mean diameter of t-tubules estimated from WGA labelling in normal myocytes was 294 ± 13 nm compared to a significantly increased diameter of 436 ± 4 nm in IDCM myocytes ($p=0.002^{**}$, n=5 donor hearts, n=5 explanted hearts, 30 t-tubules measured for each heart). Similarly, the mean diameter of t-tubules estimated from dystrophin labelling in donor myocytes was 314 ± 6 nm, significantly smaller than the 417 ± 17 nm in the diseased myocytes ($p=0.004^{**}$, n=5 donor hearts, n=5 explanted hearts, 30 t-tubules measured for each heart).

Super resolution microscopy with ~30 nm resolution was subsequently utilised to resolve the spatial distribution of WGA and dystrophin within t-tubules (Figure 1E). This revealed WGA was located predominately within the t-tubule lumen while dystrophin appear to be restricted to the t-tubular intracellular surface. In disease, t-tubule diameters were noticeably larger, an expansion that appeared to be associated with the increased WGA-positive proteins within the lumen. FWHM measurement of super resolution images confirmed findings from confocal demonstrating a significant broadening of WGA-labelled t-tubules in diseased hearts (Figure 1G). Super resolution microscopy of dystrophin labelling showed a similar significant increase in t-tubule widths in the failing hearts (Figure 1G). Note the double row of dystrophin is clearly resolved allowing the t-tubule widths to be measured by fitting a Gaussian to each line of dystrophin and estimating the outside edge of the labelling from respective FWHM estimates (see Supplementary Figure 2).

Western blotting and mass spectrometry

Western blotting was used to probe LV homogenates for WGA-positive proteins (Figure 2A). This analysis demonstrated a 1.7 fold elevation in WGA-positive proteins in IDCM samples measured by integrating total lane intensity (Figure 2B). In particular a ~140 kDa band was elevated 5.7 fold in diseased hearts (Figure 2C) which was subsequently excised and subjected to trypsin digest and tandem mass spectrometry to identify candidate glycoproteins which revealed Col-VI[39] as the only candidate. Subsequent western blots probed with an anti Col-VI antibody confirmed the ~140 kDa band as Col-VI. Col-VI was elevated 2.4 fold in failing hearts (Figure 2E) with no apparent relationship between patient age or sex (see Supplementary Figure 5). The ratio of WGA to Col-VI intensity was then calculated for the 140 kDa band to be elevated 3.2 fold in the IDCM samples indicating increased glycan content of Col-VI in disease (Figure G). We initially attempted to probe for Col-VI and WGA positive proteins in the same blot but this resulted in an absence of Col-VI labelling. A similar result was obtained from confocal imaging of the tissue (see Supplementary Data Figure 4). This result suggests steric hindrance by WGA prevents detection of Col-VI and is further evidence that WGA and Col-VI antibodies bind to the same protein target.

Col-VI alpha chain analysis

Our original LC MS/MS analysis identified α2(VI) chain within the 140 kDa WGA positive band. However the Col-VI antibody used in western blotting is raised against full length α1(VI) chain. To unambiguously determine which Col-VI alpha chain is present within the 140 kDa WGA positive region the material from this region was re-assessed using a higher sensitivity LC MS/MS analysis. This investigation was able identify between 100-200 unique proteins within the 140 kDa region in SDS PAGE gels from five normal donor hearts and 5 IDCM hearts. For each heart, three alpha chains were detected: α1(VI), α2(VI), and α3(VI). From the LC MS/MS data the approximate molar ratios of the alpha chains were calculated by normalising to α1(VI) chain intensity values. For normal donor hearts this gave a ratio of 0.92 ± 0.4 for α2(VI), and 0.32 ± 0.08 for α3(VI). IDCM hearts had a ratio of 0.96 ± 0.08 for α2(VI), and 0.56 ± 0.08 for α3(VI) (Supplementary Figure 5).

Col-VI and dystrophin labelling of t-tubules

Confocal imaging revealed Col-VI labelling area was significantly increased in heart failure particularly in the interstitial space between myocytes (Figure 3A, B & C). Col-VI had a similar distribution to WGA in the extracellular matrix, cell surface and t-tubules (Figure 3D & E). Larger donor t-tubules labelled for Col-VI also appeared to be flanked by dystrophin labelling similar to that seen for WGA (Figure 3D insert). However, again the resolution limit prevented us from resolving the distribution of these labels within the smaller tubules. In diseased hearts Col-VI labelling was noticeably increased including within the lumen of hypertrophied t-tubules that were clearly flanked by double rows of dystrophin labelling (Figure 3E insert). The distribution of t-tubules widths was assessed from confocal imaging of Col-VI labelling in 150 donor t-tubules (from 5 hearts) and 210 t-tubules from IDCM samples (from 21 regions in 7 hearts) and data are presented in Figure 1F. This analysis demonstrates that Col-VI has an increased width and larger distribution of sizes in diseased t-tubules consistent with our findings for WGA. The mean diameter of Col-VI t-tubules in donor myocytes was 272 ± 15 nm compared to significantly increased diameter of 328 ± 11 nm in IDCM myocytes (p= 0.03*, n=5 donor hearts, n=7 explanted hearts).

Super resolution microscopy resolved the distributions of Col-VI and dystrophin, particularly in the smaller t-tubules (Figure 3G & H). These images confirmed the presence of Col-VI within the tubular lumen with a noticeable accumulation within the hypertrophied t-tubules in diseased hearts (Figure 3G & H inserts). FWHM measurements demonstrated a significant increase in the distribution of Col-VI within the t-tubules in heart failure relative to donor hearts.

Col-IV, Col-III, and Col-I labelling of t-tubules

Confocal imaging of tissue sections identified that all three of these additional collagens were also present within the t-tubules and that the label diameter increased significantly in t-tubules from heart failure patients (Figure 4). The mean diameter of Col-IV t-tubules in donor myocytes was 251 ± 17 nm compared to 314 ± 20 nm in IDCM myocytes (p= 0.04*, n=5 donor hearts, n=5 explanted hearts, 30 t-tubules measured for each heart). The mean diameter of Col-III t-tubules in donor myocytes was 256 ± 10 nm compared to 396 ± 20 nm in IDCM myocytes (p= 0.003*, n as above). The mean diameter of Col-I t-tubules in donor myocytes was 266 ± 12 nm compared to 392 ± 33 nm in IDCM myocytes (p= 0.01*, n as above). Super resolution microscopy confirmed this finding (Figure 5). The total interstitial area labelled by Col-IV, Col-III, and Col-I was assessed between normal donor and IDCM hearts (Figure 6). This demonstrated a significant increase in area labelled by Col-I in heart

failure samples but not Col-IV and Col-III (Figure 6). As additional test of the presence of t-tubule collagen, tissue sections were probed with a non-antibody based method using the collagen-binding protein CNA35-mAmertrine. CNA35-mAmertrine is a recombinant protein based on collagen adhesion protein from the bacteria Staphylococcus aureus and the fluorescence protein mAmertrine[40]. Confocal imaging of this labelling also revealed positive labelling of t-tubules including increased diameter of t-tubules in heart failure (Supplementary Figure 6).

Fiboroblasts and Col-VI

To determine if fibroblast were a likely source of the increased Col-VI in heart failure the tissue density (number per unit area) of Col-VI positive fibroblasts were estimated in 5 normal donor hearts and 5 IDCM hearts (Figure 7). This analysis demonstrated a significant ~40% increase in the tissue density of fibroblasts positive to Col-VI in the failing heart. In two of the IDCM hearts we also observed several myocytes in which fibroblast filopodia projected into the lumen of larger t-tubules (Figure 7E-H).

Discussion

The data presented suggest a novel hypothesis that directly links fibrosis of the failing heart with cardiac myocyte t-tubule remodelling. Western blots demonstrate a 2.4 fold increase in Col-VI, which was consistent with significant increase in interstitial labelling measured with confocal microscopy. This increase seen in Col-VI is also consistent with increases in total collagen previously reported for IDCM[41–43]. Collagen accumulation is the major hall mark of fibrosis and the mechanisms driving changes in these classical fibrillar collagens[44] are also likely to drive the increase of Col-VI particularly as interstitial fibroblasts appear to be the major source of this collagen[45]. This is further supported by an increased tissue density of Col-VI positive fibroblasts that we have documented in IDCM hearts. Particularly intriguing is the discovery of fibroblast filopodia within the lumen of some of the enlarged t-tubules indicating a possible role in depositing the increased t-tubule Col-VI in heart failure. Both confocal and super resolution data demonstrate that this increased labelling is associated with an accumulation of Col-VI within the t-tubular lumen. Analysis of the super resolution images demonstrates a 1.6 fold increase in the Col-VI width in diseased t-tubules (231 nm compared to 370 nm). If we assume the t-tubules are cylindrical and use Archimedes geometry we calculate a volume increase of 2.6 fold, very similar to the protein expression data ratio of 2.4. Expansion of Col-VI within t-tubules is associated with displacement of the t-tubular membrane as demonstrated by concomitant widening of t-tubules when assessed from the membrane associated labelling of dystrophin. We have previously modelled that lateral disruption of cardiac junctions on the order of ~10 nm is sufficient to substantially reduce activation of the calcium release[15]. The changes in t-tubular structure we have documented are on the order of ~100 nm and could contribute to the distorted junctional structure previously described by EM[46].

Col-VI is a heterotrimeric molecule with a 1:1:1 ratio of: α1(VI), α2(VI), and α3(VI) chains that assembles into a tetramer, which upon secretion align non-covalently end to end, forming microfibrils in the ECM[32,47]. More recently an additional three novel alpha chains: α4(VI), α5(VI), and α6(VI) homologous to α3(VI) were discovered[4849]. Our LC-MS/MS analysis identified only α1(VI), α2(VI), and α3(VI) chains in the 140 kDa region positive to α1(VI) chain antibody. It is possible that other Col-VI alpha chains are present in our samples outside the 140 kDa region analysed, particularly as western blots to α6(VI) chain have

previously detected a 55 kDa band in human heart[50]. The mass spectrometry data also indicates the amount of α3(VI) is approximately half that of α1(VI) and α2(VI) indicating the possible involvement of another alpha chain such as α6(VI), which has been shown to have t-tubular location in both skeletal[51] and cardiac muscle (see immunohistochemistry images for antibody HPA045239 at: http://www.proteinatlas.org which exhibit a striated appearance consistent with t-tubular localisation)[52].

Interestingly, mutations in Col-VI are associated with Ulrich congenital muscular dystrophy and Bethlam myopathy indicating an important functional role in muscle[32]. Increased production of Col-VI fibrils by myofibroblasts/fibroblasts could contribute to the distortion in t-tubular structure documented here[44,45]. Furthermore, our finding of a 3.2 fold increase in WGA binding to Col-VI in heart failure indicates a possible increase in glycosylation that may change fibrils. Pertinently, glycosylation of hydroxylysines of individual α chains is essential for formation of mature tetramers[39]. Functionally, Col-VI is thought to provide a structural link between myocyte basal lamina and the interstitial matrix [32]. The fact that both mutations in Col-VI and dystrophin can result in muscular dystrophy[29,32] suggests these molecules are components of the same complex. This is supported by our finding that WGA binds to Col-VI and that this lectin has been used to purify dystrophin from the sarcolemma[27]. Our super resolution images are consistent with this idea demonstrating on the nano-scale that Col-VI adjacent to the sarcolemma is mirrored by a similar pattern in dystrophin. Furthermore, biglycan can bind both Col-VI and the DGC[53–55] indicative of a direct mechanical linkage. A proposed model of Col-VI and the DGC organisation in cardiac myocytes is presented in Figure 8.

Dystrophin links to both the actin and microtubule cytoskeleton [56,57] which in turn links to the L-type Ca^{2+} channel[58]. Potentially increased deposition of Col-VI places stress on the dystrophin complex distorting the myocyte cytoskeleton and displacing the alignment of the L-type Ca^{2+} channel with the ryanodine receptor within the cardiac junction. This proposition is consistent with defects in the MDX mouse that lacks functional dystrophin. The L-type calcium channels in this animal lose their ability to regulate mitochondrial activity through disruption of the cardiac myocyte cytoskeleton[58]. Furthermore, in heart failure these animals display an abnormal or prolonged cardiac Ca^{2+} release[59]. Moreover, a muscular dystrophy patient with a mutation in the α6(VI) chain had greatly reduced L-type Ca^{2+} channel and ryanodine receptor labelling[60].

Another aspect of the increased t-tubule collagen that we observe relates to the observation of geometrical deformations of t-tubules in contracting myocytes[61]. This strain-transfer has been proposed to be important for stretch-activated signaling at the t-tubule membrane as well as luminal volume exchange. The increased collagen content in heart failure would be expected to lead to a stiffening of the t-tubules and reduced strain transfer in analogy to the stiffening of heart tissue from interstitial fibrosis.

A previous study of Col-VI in human heart failure also demonstrated increased interstitial labelling but, in contrast to our results, noted only an occasion presence of t-tubule labelling[62]. We suspect methodological differences may account for the difference. For example, even moderate over-fixation of tissue can result in loss of Col-VI labelling at t-tubules. This would reduce label density preferentially reducing the contrast of smaller (or higher frequency) structures, such as t-tubules. Visualisation of faintly labelled t-tubules could also be adversely effected by lens numerical aperture and a low refractive index of the

mounting medium, experimental details that were not reported for this previous study on Col-VI in the heart.

Subsequently we examined if the t-tubules contained the basement collagen type IV and the fibrillar collagens type I and III. This analysis demonstrated all three of these collagens were present within the t-tubules, as demonstrated by confocal microscopy and confirmed by higher contrast super resolution microscopy. Furthermore, in failing hearts the dilated t-tubules identified from dystrophin labelling also had wider labelling pattern for these collagens. This data suggest that these collagens may also contribute to t-tubule remodelling in heart failure, although only a significant increase in interstitial labelling area was documented for Col-I.

In agreement with our findings Kostin et al [12] have reported presence of Col-IV within the t-tubules of the human heart. However we could not find any reports for the presence of Col-I and Col-III within t-tubules. Although, a previous study reported fine “circumferential” collagen fibres stained by picrosirius red that were perpendicular to the myocyte long axis with regular spacing of 2 μm. Some of these fibres may in fact have been t-tubule collagen similar to what we observe. Interestingly, the authors noted that these collagen fibres were difficult to observe and required increased gain on the confocal system. The difficulties in observing faint t-tubule collagen labelling against a background of intense interstitial labelling have probably resulted in the presence of collagen within the t-tubules being largely overlooked.

Limitations and future directions

An inherent limitation in the current study is that we have examined end-stage human heart failure. It is therefore not possible to determine if changes in collagens are a cause or consequence of t-tubular remodelling. The time course of changes in collagens, t-tubular structure, Ca^{2+} handling and contractile function, in response to a suitable intervention would be required to thoroughly test our new hypothesis. However, we believe we have identified a novel potential mechanism that could link tissue level fibrosis with nanoscale disruption of myocyte structure and function that warrants further investigation. In any case, the presence of several collagens and their change in failure that we show here should be considered in continuing attempts to improve the understanding of t-tubule turnover, function and loss in cardiac myocytes. For example, an over-expression model of Col-VI in the mouse could be developed to test consequences on t-tubule remodelling. Observations with an existing Col-VI knock-out mouse model are consistent with our hypothesis. Luther and colleagues reported that knock-out animals are paradoxically protected from myocardial infarction as demonstrated by improved ejection fraction, and reduced infarct size relative to wild type animals[63]. Although these authors did not examine t-tubule structure we speculate that the absence of functional Col-VI protects these animals from t-tubular remodelling providing at least some of the observed protection. Supporting this hypothesis, t-tubular changes also appear to be an important feature of ischemic heart failure[6,7]. Furthermore, beta blockade with carvedilol reduces both fibrosis[64] and t-tubule remodelling[65].

Funding

Research funding was provided by the Auckland Medical Research Foundation and the Health Research Council (grant 12/240 to CS) of New Zealand.

Acknowledgements

We are grateful to Auckland City Hospital, St Vincent's Hospital and their staff for assistance in obtaining tissue. We thank transplant recipients, and donor families for donating tissue that enabled this study.

Conflict of Interest

None

References

1. Orchard C, Brette F. t-tubules and sarcoplasmic reticulum function in cardiac ventricular myocytes. *Cardiovasc Res* 2008;**77**:237–244.
2. Bers D. Cardiac excitation–contraction coupling. *Nature* 2002;**415**:198–205.
3. Guo A, Zhang C, Wei S, Chen B, Song L-S. Emerging mechanisms of T-tubule remodelling in heart failure. *Cardiovasc Res* 2013;**98**:204–215.
4. Franzini-Armstrong C, Protasi F, Ramesh V. Shape, size, and distribution of Ca(2+) release units and couplons in skeletal and cardiac muscles. *Biophys J* 1999;**77**:1528–1539.
5. Song L-S, Sobie E a, McCulle S, Lederer WJ, Balke CW, Cheng H. Orphaned ryanodine receptors in the failing heart. *Proc Natl Acad Sci U S A* 2006;**103**:4305–4310.
6. Louch WE, Mørk HK, Sexton J, Strømme T a, Laake P, Sjaastad I, Sejersted OM. T-tubule disorganization and reduced synchrony of Ca2+ release in murine cardiomyocytes following myocardial infarction. *J Physiol* 2006;**574**:519–533.
7. Heinzel FR, Bito V, Biesmans L, Wu M, Detre E, Wegner F von, Claus P, Dymarkowski S, Maes F, Bogaert J, Rademakers F, D'hooge J, Sipido K. Remodeling of T-tubules and reduced synchrony of Ca2+ release in myocytes from chronically ischemic myocardium. *Circ Res* 2008;**102**:338–346.
8. Wei S, Guo A, Chen B, Kutschke W, Xie Y-P-P, Zimmerman K, Weiss RM, Anderson ME, Cheng H, Song L-S-S. T-tubule remodeling during transition from hypertrophy to heart failure. *Circ Res* 2010;**107**:520–531.
9. Sacconi L, Ferrantini C, Lotti J, Coppini R, Yan P, Loew LM, Tesi C, Cerbai E, Poggesi C, Pavone FS. Action potential propagation in transverse-axial tubular system is impaired in heart failure. *Proc Natl Acad Sci U S A* 2012;**109**:5815–5819.
10. Crocini C, Coppini R, Ferrantini C, Yan P, Loew LM, Tesi C, Cerbai E, Poggesi C, Pavone FS, Sacconi L. Defects in T-tubular electrical activity underlie local alterations of calcium release in heart failure. *Proc Natl Acad Sci U S A* 2014;**111**:15196–15201.
11. Ibrahim M, Terracciano CM. Reversibility of T-tubule remodelling in heart failure: Mechanical load as a dynamic regulator of the T-tubules. *Cardiovasc Res* 2013;**98**:225–232.
12. Kostin S, Scholz D, Shimada T, Maeno Y, Mollnau H, Hein S, Schaper J. The internal and external protein scaffold of the T-tubular system in cardiomyocytes. *Cell Tissue Res* 1998;**294**:449–460.
13. Heling A, Kostin S, Maeno Y, Hein S, Devaux B, Bauer E, Klo W, Schlepper M, Schaper W, Schaper J. Extracellular Proteins in Failing Human Myocardium. *Circ Res* 2000;846–853.
14. Louch W. Reduced synchrony of Ca2+ release with loss of T-tubules—a comparison to Ca2+ release in human failing cardiomyocytes. *Cardiovasc Res* 2004;**62**:63–73.

15. Cannell MB, Crossman DJ, Soeller C. Effect of changes in action potential spike configuration, junctional sarcoplasmic reticulum micro-architecture and altered t-tubule structure in human heart failure. *J Muscle Res Cell Motil* 2006;**27**:297–306.

16. Lyon AR, MacLeod KT, Zhang Y, Garcia E, Kanda GK, Lab MJ, Korchev YE, Harding SE, Gorelik J. Loss of T-tubules and other changes to surface topography in ventricular myocytes from failing human and rat heart. *Proc Natl Acad Sci U S A* 2009;**106**:6854–6859.

17. Crossman DJ, Ruygrok PR, Soeller C, Cannell MB. Changes in the organization of excitation-contraction coupling structures in failing human heart. *PLoS One* 2011;**6**:e17901.

18. Crossman DJ, Young AA, Ruygrok PN, Nason GP, Baddelely D, Soeller C, Cannell MB. t-tubule disease: Relationship between t-tubule organization and regional contractile performance in human dilated cardiomyopathy. *J Mol Cell Cardiol* Elsevier B.V.; 2015;**84**:170–178.

19. Hohendanner F, Ljubojević S, MacQuaide N, Sacherer M, Sedej S, Biesmans L, Wakula P, Platzer D, Sokolow S, Herchuelz A, Antoons G, Sipido K, Pieske B, Heinzel FR. Intracellular dyssynchrony of diastolic cytosolic [Ca^{2+}] decay in ventricular cardiomyocytes in cardiac remodeling and human heart failure. *Circ Res* 2013;**113**:527–538.

20. Zhang C, Chen B, Guo A, Zhu Y, Miller JD, Gao S, Yuan C, Kutschke W, Zimmerman K, Weiss RM, Wehrens XHT, Hong J, Johnson FL, Santana LF, Anderson ME, Song L-S. Microtubule-mediated defects in junctophilin-2 trafficking contribute to myocyte T-tubule remodeling and Ca2+ handling dysfunction in heart failure. *Circulation* 2014;**129**:1742–1750.

21. Wu C-YC, Chen B, Jiang Y-P, Jia Z, Martin DW, Liu S, Entcheva E, Song L-S, Lin RZ. Calpain-dependent cleavage of junctophilin-2 and T-tubule remodeling in a mouse model of reversible heart failure. *J Am Heart Assoc* 2014;**3**:e000527.

22. Guo A, Zhang X, Iyer VR, Chen B, Zhang C, Kutschke WJ, Weiss RM, Franzini-Armstrong C, Song L-S. Overexpression of junctophilin-2 does not enhance baseline function but attenuates heart failure development after cardiac stress. *Proc Natl Acad Sci U S A* 2014;**111**:12240–12245.

23. Oort RJ van, Garbino A, Wang W, Dixit SS, Landstrom AP, Gaur N, Almeida AC De, Skapura DG, Rudy Y, Burns AR, Ackerman MJ, Wehrens XHT. Disrupted junctional membrane complexes and hyperactive ryanodine receptors after acute junctophilin knockdown in mice. *Circulation* 2011;**123**:979–988.

24. Caldwell JL, Smith CE, Taylor RF, Kitmitto A, Eisner D a, Dibb KM, Trafford AW. Dependence of cardiac transverse tubules on the BAR domain protein amphiphysin II (BIN-1). *Circ Res* 2014;**115**:986–996.

25. Hong T, Yang H, Zhang S-S, Cho HC, Kalashnikova M, Sun B, Zhang H, Bhargava A, Grabe M, Olgin J, Gorelik J, Marbán E, Jan LY, Shaw RM. Cardiac BIN1 folds T-tubule membrane, controlling ion flux and limiting arrhythmia. *Nat Med* 2014;**20**:624–632.

26. Ibrahim M, Siedlecka U, Buyandelger B, Harada M, Rao C, Moshkov A, Bhargava A, Schneider M, Yacoub MH, Gorelik J, Knöll R, Terracciano CM. A critical role for Telethonin in regulating t-tubule structure and function in the mammalian heart. *Hum Mol Genet* 2013;**22**:372–383.

27. Campbell KP, Kahl SD. Association of dystrophin and an integral membrane glycoprotein. *Nature* 1989;**338**:259–262.

28. Verhaert D, Richards K, Rafael-Fortney JA, Raman S V. Cardiac involvement in patients with muscular dystrophies magnetic resonance imaging phenotype and

genotypic considerations. *Circ Cardiovasc Imaging* 2011;**4**:67–76.

29. Lapidos K a., Kakkar R, McNally EM. The dystrophin glycoprotein complex: signaling strength and integrity for the sarcolemma. *Circ Res* 2004;**94**:1023–1031.
30. Vatta M, Stetson SJ, Perez-verdia A, Entman ML, Noon GP, Torre-amione G, Bowles NE, Towbin JA. Molecular remodelling of dystrophin in patients with end-stage cardiomyopathies and reversal in patients on assistance-device therapy. *Lancet* 2002;**359**:936–941.
31. Kaprielian RR, Stevenson S, Rothery SM, Cullen MJ, Severs NJ. Distinct patterns of dystrophin organization in myocyte sarcolemma and transverse tubules of normal and diseased human myocardium. *Circulation* 2000;**101**:2586–2594.
32. Allamand V, Briñas L, Richard P, Stojkovic T, Quijano-Roy S, Bonne G. ColVI myopathies: where do we stand, where do we go? *Skelet Muscle* BioMed Central Ltd; 2011;**1**:30.
33. Soeller C, Cannell MB. Cardiac rat myocytes by 2-photon microscopy and digital image–processing techniques. *Circ Res* 1999;**84**:266–275.
34. Camelliti P, Borg TK, Kohl P. Structural and functional characterisation of cardiac fibroblasts. *Cardiovasc Res* 2005;**65**:40–51.
35. Crossman DJ, Hou Y, Jayasinghe I, Baddeley D, Soeller C. Combining confocal and single molecule localisation microscopy: A correlative approach to multi-scale tissue imaging. *Methods* Elsevier Inc.; 2015;**In Press**.
36. Baddeley D, Crossman D, Rossberger S, Cheyne JE, Montgomery JM, Jayasinghe ID, Cremer C, Cannell MB, Soeller C. 4D super-resolution microscopy with conventional fluorophores and single wavelength excitation in optically thick cells and tissues. *PLoS One* 2011;**6**:e20645.
37. Tokunaga M, Imamoto N, Sakata-Sogawa K. Highly inclined thin illumination enables clear single-molecule imaging in cells. *Nat Methods* 2008;**5**:159–161.
38. Baddeley D. Visualization of localization microscopy data. *Microsc Microanal* 2010;**16**:64–72.
39. Sipilä L, Ruotsalainen H, Sormunen R, Baker NL, Lamandé SR, Vapola M, Wang C, Sado Y, Aszodi A, Myllylä R. Secretion and assembly of type IV and VI collagens depend on glycosylation of hydroxylysines. *J Biol Chem* 2007;**282**:33381–33388.
40. Aper SJA, Spreeuwel ACC Van, Turnhout MC Van, Linden AJ Van Der, Pieters PA, Zon NLL Van Der, La Rambelje SL De, Bouten CVC, Merkx M. Colorful protein-based fluorescent probes for collagen imaging. *PLoS One* 2014;**9**:1–21.
41. Hamdani N, Borbély A, Veenstra SPGR, Kooij V, Vrydag W, Zaremba R, Remedios C Dos, Niessen HWM, Michel MC, Paulus WJ, Stienen GJM, Velden J Van Der. More severe cellular phenotype in human idiopathic dilated cardiomyopathy compared to ischemic heart disease. *J Muscle Res Cell Motil* 2010;**31**:289–301.
42. Abdullah OM, Drakos SG, Diakos N a., Wever-Pinzon O, Kfoury AG, Stehlik J, Selzman CH, Reid BB, Brunisholz K, Verma DR, Myrick C, Sachse FB, Li DY, Hsu EW. Characterization of diffuse fibrosis in the failing human heart via diffusion tensor imaging and quantitative histological validation. *NMR Biomed* 2014;**27**:1378–1386.
43. Gunja-Smith Z, Morales a R, Romanelli R, Woessner JF. Remodeling of human myocardial collagen in idiopathic dilated cardiomyopathy. Role of metalloproteinases and pyridinoline cross-links. *Am J Pathol* 1996;**148**:1639–1648.
44. Segura AM, Frazier OH, Buja LM. Fibrosis and heart failure. *Heart Fail Rev* 2014;**19**:173–185.
45. Zou Y, Zhang R-Z, Sabatelli P, Chu M-L, Bönnemann CG. Muscle interstitial

fibroblasts are the main source of collagen VI synthesis in skeletal muscle: implications for congenital muscular dystrophy types Ullrich and Bethlem. *J Neuropathol Exp Neurol* 2008;**67**:144–154.

46. Zhang H-B, Li R-C, Xu M, Xu S-M, Lai Y-S, Wu H-D, Xie X-J, Gao W, Ye H, Zhang Y-Y, Meng X, Wang S-Q. Ultrastructural uncoupling between T-tubules and sarcoplasmic reticulum in human heart failure. *Cardiovasc Res* 2013;**98**:269–276.
47. Engvall E, Hessle H, Klier G. Molecular assembly, secretion, and matrix deposition of type VI collagen. *J Cell Biol* 1986;**102**:703–710.
48. Fitzgerald J, Rich C, Zhou FH, Hansen U. Three novel collagen VI chains, α4(VI), α5(VI), and α6(VI). *J Biol Chem* 2008;**283**:20170–20180.
49. Gara SK, Grumati P, Urciuolo A, Bonaldo P, Kobbe B, Koch M, Paulsson M, Wagener R. Three novel collagen VI chains with high homology to the α3 chain. *J Biol Chem* 2008;**283**:10658–10670.
50. Holden P, Moscibrocki C, Fitzgerald J. Characterization Of The Alpha 6 Chain Of Collagen VI Collagen : Implications For Macromolecular Assembly And Function ORS. *Transactions of the annual meeting of the Orthopaedic Research Society* 2014;**59**:1237.
51. Holden P, Moscibrocki C, Fitzgerald J. Unique distribution of the α6 chain of collagen VI in skeletal muscle. *Transactions of the annual meeting of the Orthopaedic Research Society* 2013;**58**:1408.
52. Uhlen M, Fagerberg L, Hallstrom BM, Lindskog C, Oksvold P, Mardinoglu A, Sivertsson A, Kampf C, Sjostedt E, Asplund A, Olsson I, Edlund K, Lundberg E, Navani S, Szigyarto CA-K, Odeberg J, Djureinovic D, Takanen JO, Hober S, Alm T, Edqvist P-H, Berling H, Tegel H, Mulder J, Rockberg J, Nilsson P, Schwenk JM, Hamsten M, Feilitzen K von, Forsberg M, et al. Tissue-based map of the human proteome. *Science (80-)* 2015;**347**:1260419–1260419.
53. Wiberg C, Heinegård D, Wenglén C, Timpl R, Mörgelin M. Biglycan organizes collagen VI into hexagonal-like networks resembling tissue structures. *J Biol Chem* 2002;**277**:49120–49126.
54. Rafii MS, Hagiwara H, Mercado ML, Seo NS, Xu T, Dugan T, Owens RT, Hook M, McQuillan DJ, Young MF, Fallon JR. Biglycan binds to α- and γ-sarcoglycan and regulates their expression during development. *J Cell Physiol* 2006;**209**:439–447.
55. Wiberg C, Hedbom E, Khairullina A, Lamandé SR, Oldberg Å, Timpl R, Mörgelin M, Heinegård D. Biglycan and Decorin Bind Close to the N-terminal Region of the Collagen VI Triple Helix. *J Biol Chem* 2001;**276**:18947–18952.
56. Renley BA, Rybakova IN, Amann KJ, Ervasti JM. Dystrophin binding to nonmuscle actin. *Cell Motil Cytoskeleton* 1998;**41**:264–270.
57. Prins KW, Humston JL, Mehta A, Tate V, Ralston E, Ervasti JM. Dystrophin is a microtubule-associated protein. *J Cell Biol* 2009;**186**:363–369.
58. Viola HM, Adams AM, Davies SMK, Fletcher S, Filipovska A, Hool LC. Impaired functional communication between the L-type calcium channel and mitochondria contributes to metabolic inhibition in the mdx heart. *Proc Natl Acad Sci U S A* 2014;**111**:E2905-14.
59. Cheng Y-J, Lang D, Caruthers SD, Efimov IR, Chen J, Wickline S a. Focal but reversible diastolic sheet dysfunction reflects regional calcium mishandling in dystrophic mdx mouse hearts. *AJP Hear Circ Physiol* 2012;**303**:H559–H568.
60. Fitzgerald J, Moscibrocki C, Lamande S, North K, Holden P. A Mutation In The Alpha 6 Chain Of Type Vi Collagen Disrupts E-c Coupling And Leads To A Lethal Muscular Dystrophy. *Transactions of the annual meeting of the Orthopaedic Research Society*

2014;**58**:527.

61. McNary TG, Bridge JHB, Sachse FB. Strain Transfer in Ventricular Cardiomyocytes to Their Transverse Tubular System Revealed by Scanning Confocal Microscopy. *Biophys J* Biophysical Society; 2011;**100**:L53–L55.
62. Mollnau H, Münkel B, Schaper J. Collagen VI in the extracellular matrix of normal and failing human myocardium. *Herz* 1995;**20**:89–94.
63. Luther DJ, Thodeti CK, Shamhart PE, Adapala RK, Hodnichak C, Weihrauch D, Bonaldo P, Chilian WM, Meszaros JG. Absence of type VI collagen paradoxically improves cardiac function, structure, and remodeling after myocardial infarction. *Circ Res* 2012;**110**:851–856.
64. Wei S, Chow LTC, Sanderson JE. Effect of carvedilol in comparison with metoprolol on myocardial collagen postinfarction. *J Am Coll Cardiol* 2000;**36**:276–281.
65. Chen B, Li Y, Jiang S, Xie Y-P, Guo A, Kutschke W, Zimmerman K, Weiss RM, Miller FJ, Anderson ME, Song L-S. β-Adrenergic receptor antagonists ameliorate myocyte T-tubule remodeling following myocardial infarction. *FASEB J* 2012;**26**:2531–2537.

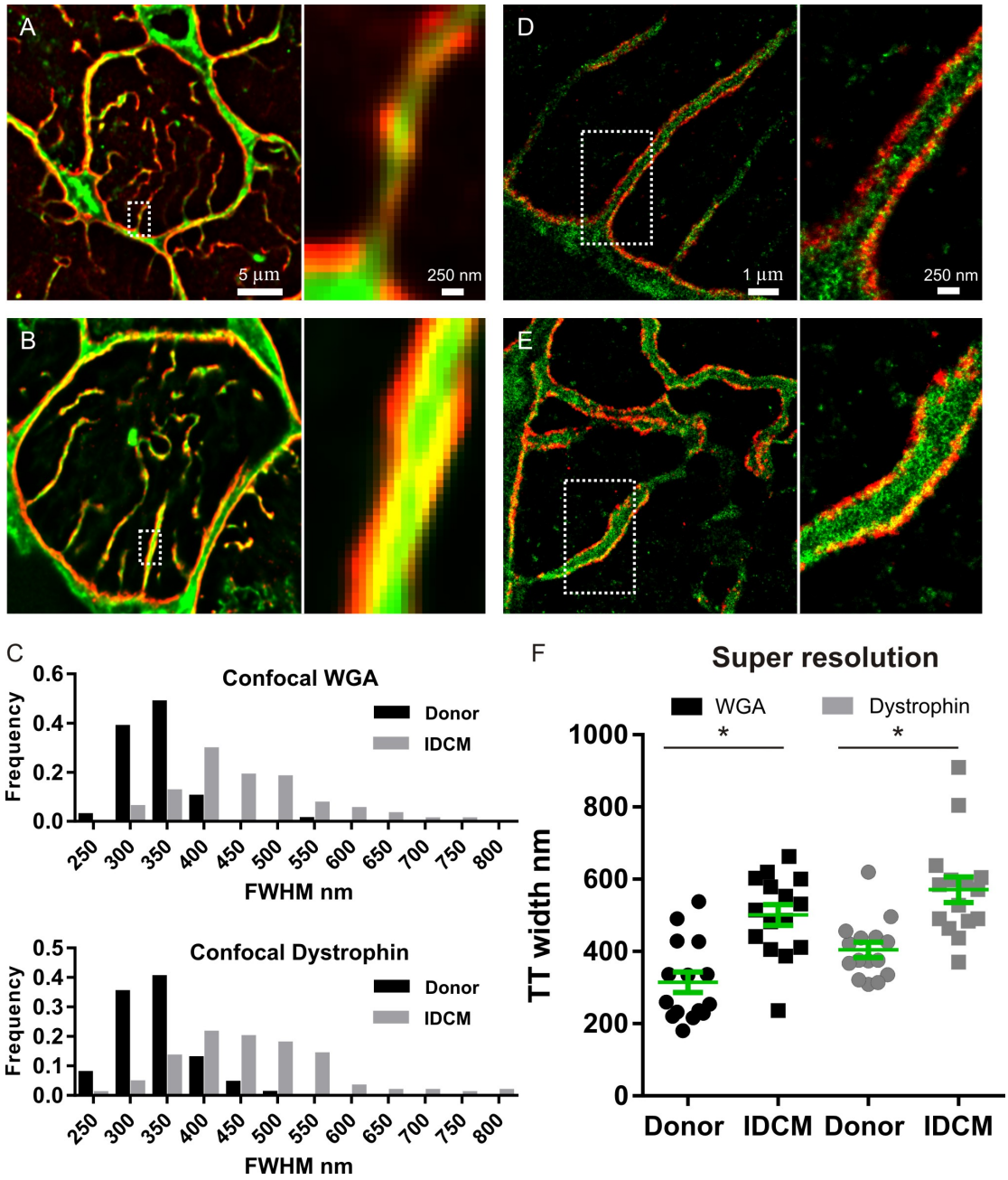

Figure 1 WGA (red) labelling increases within the lumen of dilated t-tubules in heart failure and is flanked by dystrophin (red) labelling. (A) Left panel shows a confocal image of a transverse myocyte from a donor patient. Right panel shows an enlargement of a t-tubule indicated by a white box. (B) Left panel shows a confocal image of a transverse myocyte from an IDCM patient. Right panel shows an enlargement of a t-tubule indicated by a white box. (C) Top panel: the distribution of t-tubule widths assessed from confocal images of WGA labelling for donor and IDCM samples. Bottom panel: the distribution of t-tubule widths assessed from confocal images of dystrophin labelling for normal and IDCM patients. N = 150 donor t-tubules from (from 5 hearts) and 150 diseased t-tubules (from 5 hearts) (D) Super resolution microscopy of t-tubules from a donor patient. Right panel: enlargement of t-tubule indicated by white box. (E) Super resolution microscopy of t-tubules from IDCM patient. Right panel: enlargement of area indicated by white box. (F) Mean t-tubule widths assessed from super resolution images of WGA and dystrophin labelling (*p<0.038 and *p=0.028 respectively from n=5 donor hearts, n=5 explanted hearts, 3 t-tubules from separate cells were measured in each heart).

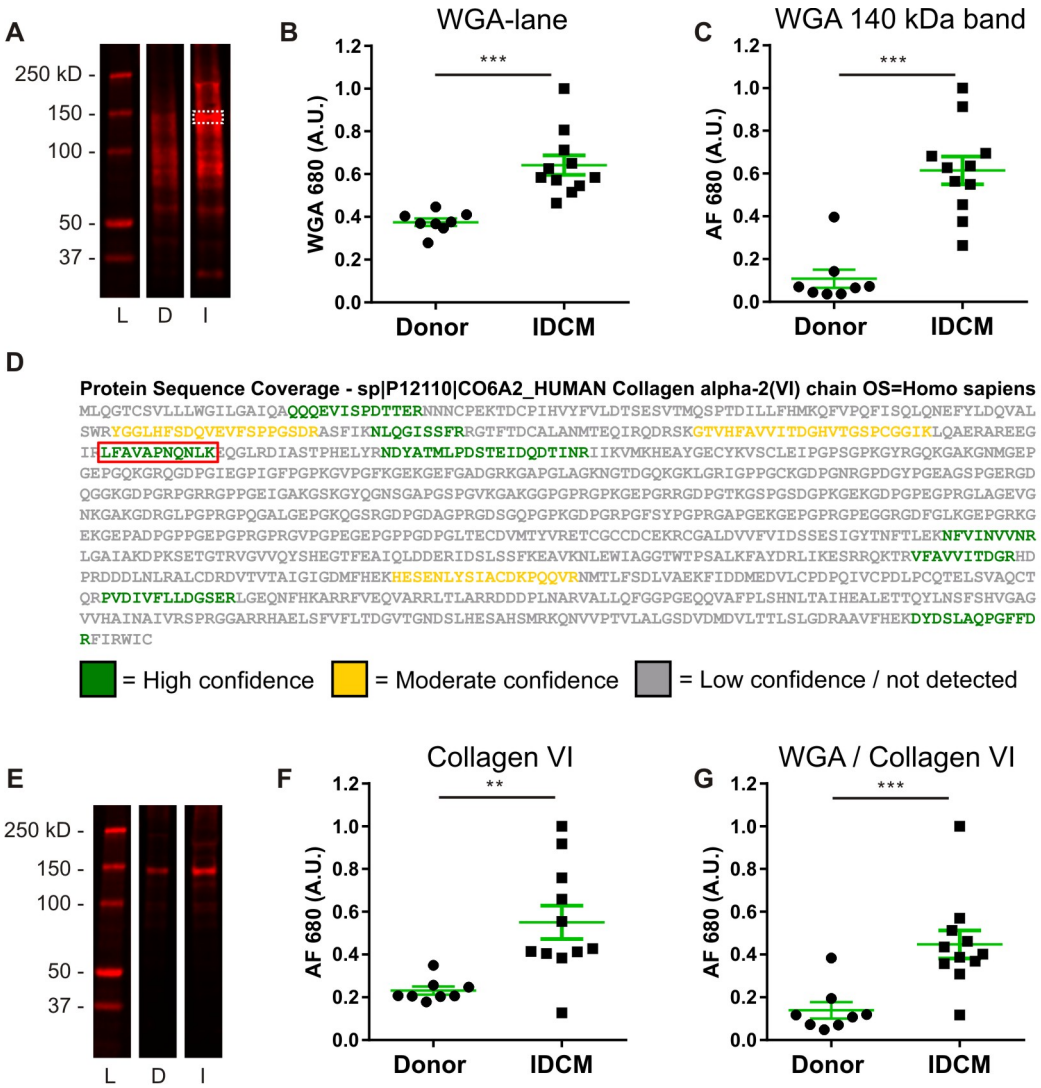

Figure 2 Proteomic analysis of WGA positive proteins in human heart failure identifies Col-VI. (A) Exemplar lanes of protein blots probed with WGA. L = ladder, D = donor sample, I = IDCM sample. (B) Mean total WGA lane intensity. A.U = arbitrary units. p=0.001***, n = 8 donor and n = 11 failing hearts. (C) Mean WGA intensity for 140 kda band indicated by white box in A. p=0.001***, n = 8 donor and n = 11 failing hearts. (D) Peptide fragments identified from Col-VI alpha-2 chain by mass spectrometry. See Supplementary Figure II for examples of peptide ionisation for sequence in red box. (E) Western blot for Col-VI. (F) Mean intensity of Col-VI in western blot. p=0.002** n = 8 donor and 11 IDCM samples. G, Ratio of WGA intensity over Col-VI intensity. P<0.001*** n = 8 donor and 11 IDCM samples.

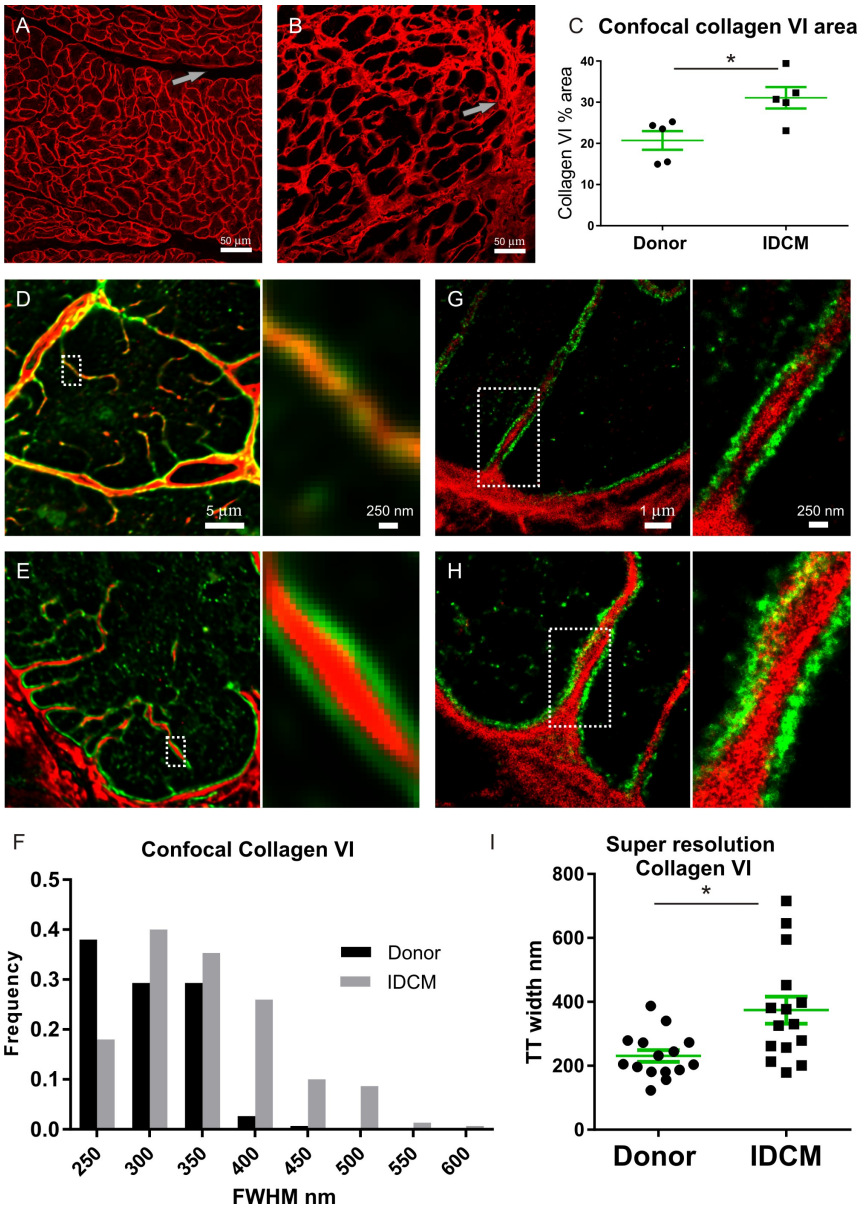

Figure 3 Col-VI labelling increases within the lumen of t-tubules in heart failure and is flanked by dystrophin labelling. Col-VI labelling in red and dystrophin in green. (A) Confocal image of ColVI in a healthy donor LV section where labelling is predominately associated with cardiac myocyte sarcolemma with interstitial spaces largely lacking label (grey arrow). (B) Confocal image of ColVI in an IDCM LV section showing a large amount of interstitial labelling (grey arrow). (C) Mean area occupied by Col-VI in donor and failing hearts. p = 0.02* n = 5 donor and 5 IDCM samples, 3 images analysed for each heart (D) Left panel shows a confocal image of a transverse myocyte from a donor. Right panel shows an enlargement of t-tubule indicated by a white box. (E) Left panel shows a confocal image of a transverse myocyte from a LV sample from IDCM patient. Right panel shows an enlargement of t-tubule indicated by a white box. (F) Distribution of t-tubule widths assessed from confocal images of Col-VI labelling. N = 150 donor t-tubules from (from 5 hearts) and 210 diseased t-tubules (from 7 hearts). (G) Super resolution microscopy of t-tubules from a normal patient. Right panel: enlargement of t-tubule indicated by white box. (H) Super resolution microscopy of t-tubules from a IDCM sample. Right panel: enlargement of area indicated by a white box. (I) Mean t-tubule widths assessed from super resolution images of Col-VI labelling. *p=0.014 from n=5 donor hearts, n=5 explanted hearts, t-tubules from 3 separate cells were measured in each heart.

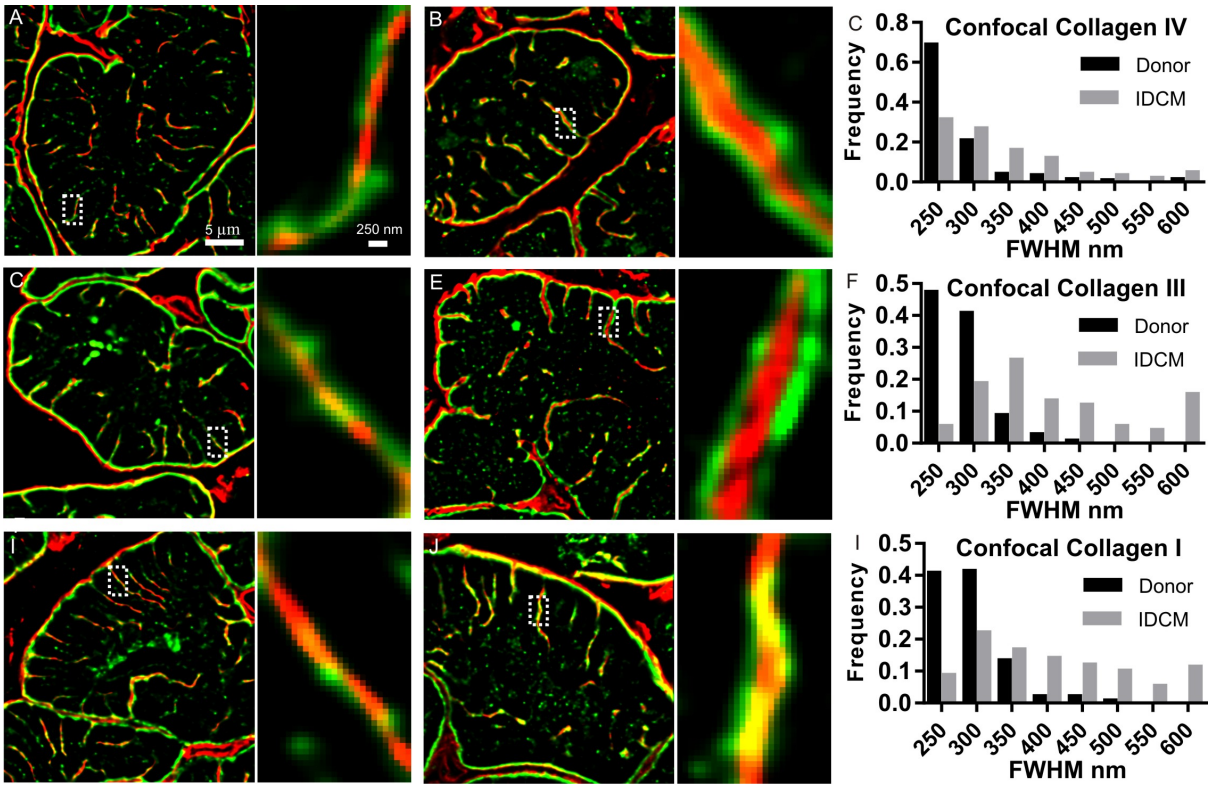

Figure 4. Confocal imaging demonstrates type IV, type III, and type I collagens are also present within the t-tubules and that diameters increase in heart failure. (A) Col-IV (red) and dystrophin (green) labelling in a transverse optical section through a myocyte from a normal donor heart (Left hand panel). Right panel shows an enlargement of a t-tubule indicated by a white box. (B) Col-IV (red) and dystrophin (green) labelling in a transverse myocyte from a IDCM patient (Left hand panel). The right panel shows an enlargement of a t-tubule indicated by a white box. (C) The distribution of t-tubule widths assessed from confocal images of Col-IV labelling for donor and IDCM samples. N = 150 donor t-tubules from (from 5 hearts) and 150 diseased t-tubules (from 5 hearts). (D) Col-III (red) and dystrophin (green) labelling in a transverse myocyte from a donor (Left hand panel). The right panel shows an enlargement of a t-tubule indicated by a white box. N same as in A. (E) Col-III (red) and dystrophin (green) labelling in a transverse myocyte from a IDCM patient (Left hand panel). Right panel shows an enlargement of t-tubule indicated by a white box. Statistical sampling as in A. (C) The distribution of t-tubule widths assessed from confocal images of Col-III labelling for donor and IDCM samples. N = 150 donor t-tubules from (from 5 hearts) and 150 diseased t-tubules (from 5 hearts). (E) Col-I (red) and dystrophin (green) labelling in a transverse myocyte from a donor (Left hand panel). The right panel shows an enlargement of a t-tubule indicated by a white box. Statistical sampling as in A. (F) Col-I (red) and dystrophin (green) labelling in a transverse myocyte from a IDCM patient (Left hand panel). Right panel shows an enlargement of t-tubule indicated by a white box. Statistical sampling as as in A. (C) The distribution of t-tubule widths assessed from confocal images of Col-I labelling for donor and IDCM samples. N = 150 donor t-tubules from (from 5 hearts) and 150 diseased t-tubules (from 5 hearts)

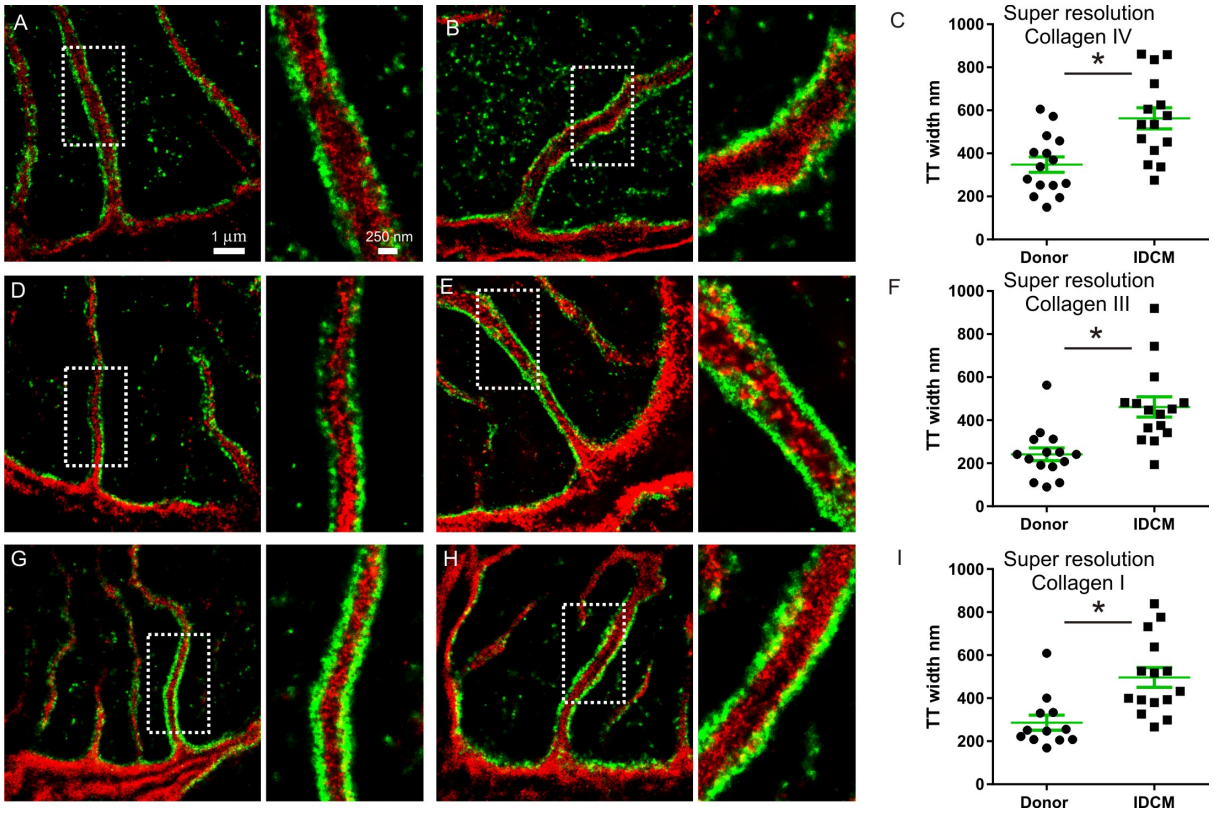

Figure 5. Super resolution microscopy confirms type IV, type III, and type I collagens are within the t-tubules and that diameters increase in heart failure. (A) Col-IV (red) and dystrophin (green) labelling in a transverse myocyte from a donor (Left hand panel).Right panel shows an enlargement of t-tubule indicated by a white box. (B) Col-IV (red) and dystrophin (green) labelling in a transverse myocyte from a IDCM patient (Left hand panel). Right panel shows an enlargement of t-tubule indicated by a white box. (C) Mean t-tubule widths assessed from super resolution images of Col-IV labelling. *p=0.02 from n=5 donor hearts, n=5 explanted hearts, 3 t-tubules from separate cells were measured in each heart. (D) Col-III (red) and dystrophin (green) labelling in a transverse myocyte from a donor (Left hand panel).Right panel shows an enlargement of t-tubule indicated by a white box. (E) Col-III (red) and dystrophin (green) labelling in a transverse myocyte from a IDCM patient (Left hand panel). Right panel shows an enlargement of the t-tubule indicated by a white box. (F) Mean t-tubule widths assessed from super resolution images of Col-III labelling. *p=0.01 from n=5 donor hearts, n=5 explanted hearts, 3 t-tubules from separate cells were measured in each heart. (G) Col-I (red) and dystrophin (green) labelling in a transverse myocyte from a donor (Left hand panel).Right panel shows an enlargement of the t-tubule indicated by a white box. N same as in A. (H) Col-I (red) and dystrophin (green) labelling in a transverse myocyte from a IDCM patient (Left hand panel). Right panel shows an enlargement of the t-tubule indicated by a white box. (I) Mean t-tubule widths assessed from super resolution images of Col-I labelling. *p=0.02 from n=5 donor hearts, n=4 explanted hearts, 3 t-tubules from separate cells were measured in each heart.

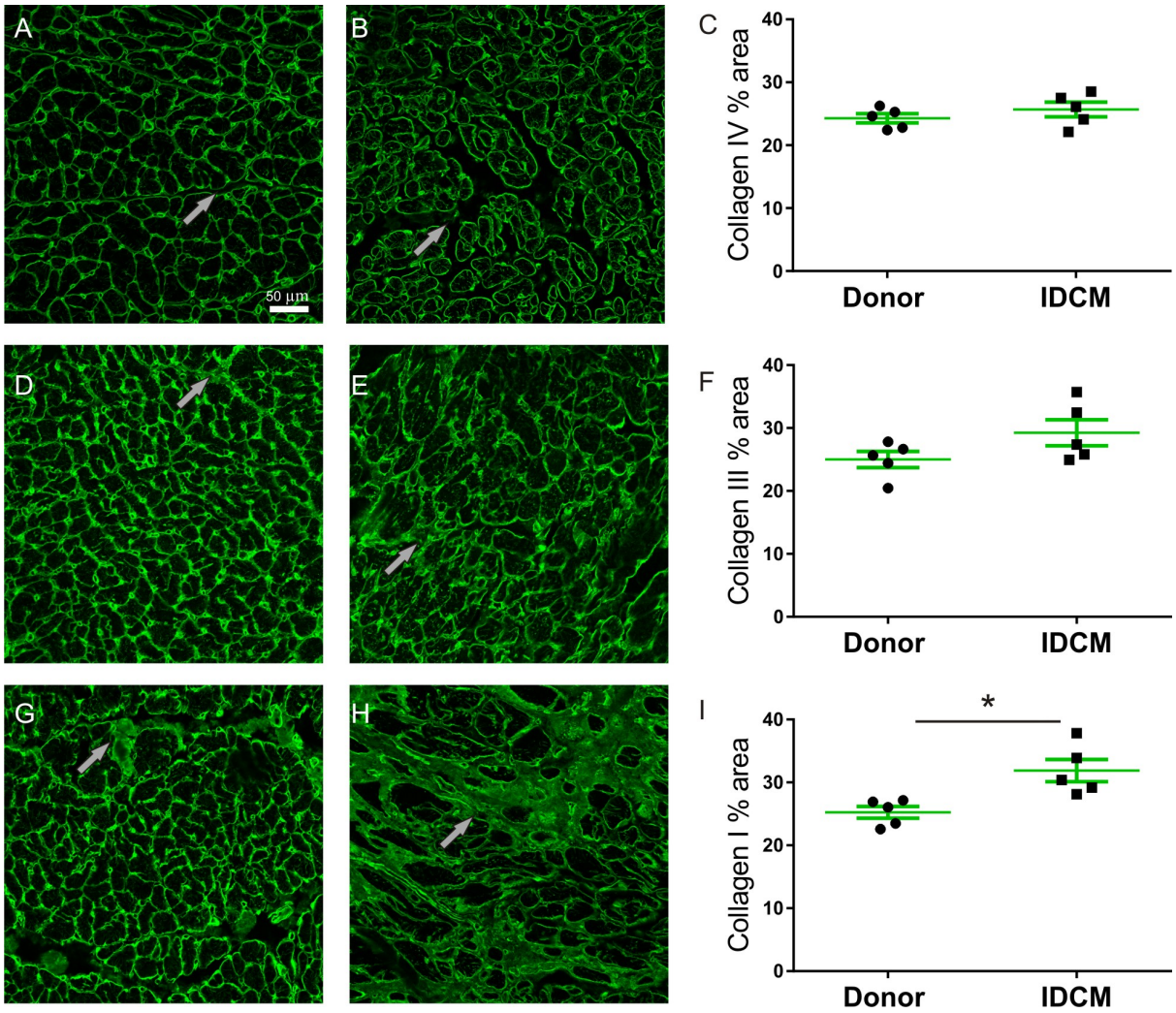

Figure 6. Confocal assessment of interstitial labelling of type IV, type III, and type I collagens in human heart failure. (A) Confocal image of Col-IV in a healthy donor LV section where labelling is associated with myocyte sarcolemma (grey arrow indicates interstitium). (B) ColVI in an IDCM LV section showing similar labelling to D (grey arrow indicates interstitium). (C) Mean area occupied by Col-IV in donor and failing hearts. p = 0.3, n = 5 donor and 5 IDCM samples, 3 images analysed for each heart. (D) Col-III in a healthy donor LV section where labelling is associated with both myocyte sarcolemma and interstitial spaces (grey arrow). (E) Col-III in an IDCM LV section showing similar labelling to D (grey arrow indicates interstitium). (F) Mean area occupied by Col-III in donor and failing hearts. p = 0.1, n same as in C. (G) Col-I in a healthy donor LV section where labelling is associated with both myocyte sarcolemma and interstitium (grey arrow). (H) Col-I in an IDCM LV showing a large increase in interstitial labelling (grey arrow). (I) Mean area occupied by Col-I in donor and failing hearts. *p = 0.03, n same as in C.

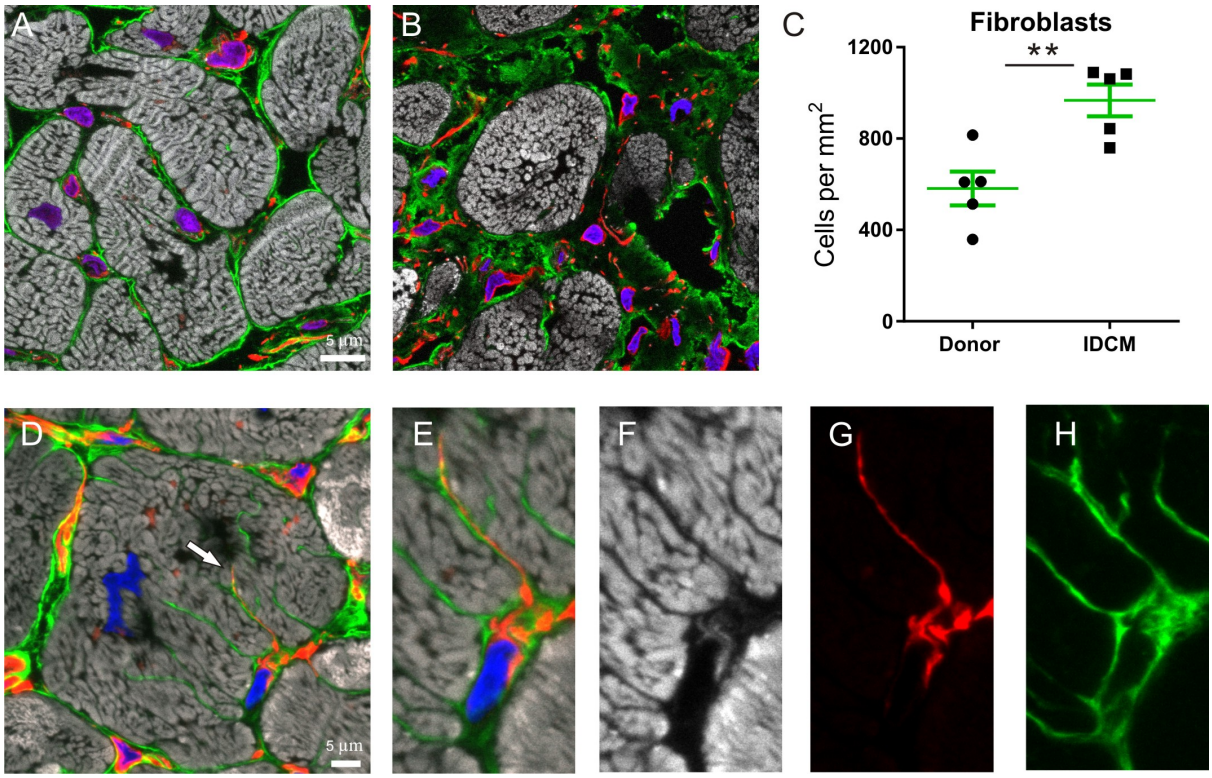

Figure 7. Increased tissue density of Col-VI positive fibroblasts in human heart failure. (A) Confocal micrograph of healthy donor section showing fibroblasts positive for Col-VI. Fibroblasts are identified from positive labelling of vimentin (red), nuclei (with DAPI signal in blue) and Col-VI (green). Phalloidin labelling of actin is shown in grey. (B) Confocal micrograph of IDCM section showing increased numbers of Col-VI positive fibroblasts per tissue area. (C) Mean tissue density of Col-VI fibroblasts in donor and failing hearts. **p < 0.01, n = 5 donor and 5 IDCM samples, 5 images analysed for each heart. (D) Confocal z-projection (from 3.3 µm axial thickness volume data) of myocyte from IDCM heart showing an enlarged t-tubule (white arrow) containing fibroblast filopodia (red). (E) Enlargement of area near white arrow in D, showing fibroblast nuclei (blue) and filopodia (red), note intracellular Col-VI in fibroblast. (F) Phalloidin labelling from E. Vimentin labelling from E. Col-VI labelling from E.

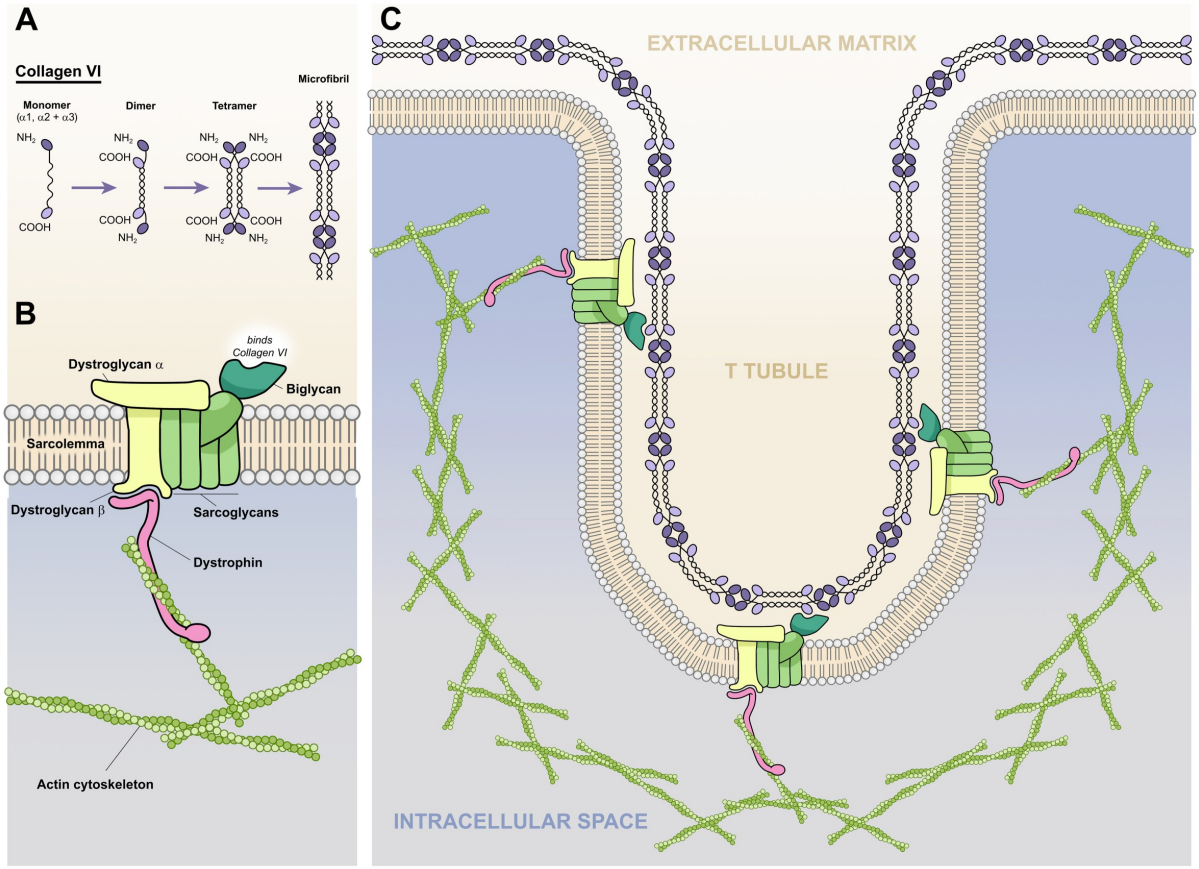

Figure 8.~~7~~ Model of Col-VI and dystrophin within the t-tubule. (A) The assembly of Col-VI into tetramers and microfibrils. (B) Dystrophin glycoprotein complex. (C) Suggested t-tubule model with Col-VI microfibrils linking to the dystrophin glycoprotein complex that in turn connects to the myocyte cytoskeleton through actin.